

Anisotropic optical trapping of ultracold erbium atoms

M. Lepers¹, J.-F. Wyart^{1,2} and O. Dulieu¹

¹*Laboratoire Aimé Cotton, CNRS/Univ. Paris-Sud/ENS-Cachan,*

*Bât. 505, Campus d'Orsay, 91405 Orsay, France** and

²*LERMA, UMR8112, Observatoire de Paris-Meudon,*

Univ. Pierre et Marie Curie, 92195 Meudon, France

(Dated: October 24, 2013)

Ultracold atoms confined in a dipole trap are submitted to a potential whose depth is proportional to the real part of their dynamic dipole polarizability. The atoms also experience photon scattering whose rate is proportional to the imaginary part of their dynamic dipole polarizability. In this article we calculate the complex dynamic dipole polarizability of ground-state erbium, a rare-earth atom that was recently Bose-condensed. The polarizability is calculated with the sum-over-state formula inherent to second-order perturbation theory. The summation is performed on transition energies and transition dipole moments from ground-state erbium, which are computed using the Racah-Slater least-square fitting procedure provided by the Cowan codes. This allows us to predict 9 unobserved odd-parity energy levels of total angular momentum $J = 5, 6$ and 7 , in the range 25000-31000 cm⁻¹ above the ground state. Regarding the trapping potential, we find that ground-state erbium essentially behaves like a spherically-symmetric atom, in spite of its large electronic angular momentum. We also find a mostly isotropic van der Waals interaction between two ground-state erbium atoms, characterized by a coefficient $C_6^{\text{iso}} = 1760$ a.u.. On the contrary, the photon-scattering rate shows a pronounced anisotropy, since it strongly depends on the polarization of the trapping light.

* maxence.lepers@u-psud.fr

I. INTRODUCTION

In the field of ultracold atomic and molecular matter, quantum gases composed of particles with a strong intrinsic permanent dipole moment, referred to as dipolar gases, have attracted a lot of interest during the last few years, as they can be manipulated by external electric or magnetic fields [1–4]. Due to the long-range and anisotropic particle-particle interactions, dipolar gases offer the possibility to produce and study highly-correlated quantum matter, which are crucial for quantum information, or for the simulation of many-body or condensed-matter physics [5, 6]. The production of ultracold heteronuclear bialkali molecules, which carry a permanent electric dipole moment, in the lowest electronic state [7, 8], the ground rovibronic [9, 10] and even hyperfine level [11], was a ground-breaking result, as it demonstrated the possibility to control both the internal and external molecular degrees of freedom [12].

Alternatively open-shell atoms possess a permanent magnetic dipole moment which is determined by their total angular momentum. The latter has the smallest possible value for alkali-metal atoms, namely $1/2$, but it can be significantly larger for transition-metal or rare-earth atoms. In the context of ultracold matter, the first Bose-Einstein condensates of highly-magnetic atoms, obtained with chromium [13, 14], were also crucial achievements. Later on, lanthanides started to draw a lot of attention: ultracold erbium atoms were produced in a magneto-optical trap in 2006 [15]. More recently Bose-Einstein condensation was reached with erbium [16] and dysprosium [17–21], and ultracold thermal samples of thulium [22, 23] and holmium were also produced. These achievements stimulated both theoretical [24–28] and experimental studies [29, 30], which complemented the work on ytterbium, the heavier (closed-shell) lanthanide element (see for example Ch. 1 of [31] and references therein).

In the present paper we theoretically investigate the optical trapping of ground-state 3H_6 erbium atoms. The efficiency of the trapping mechanism relies on the knowledge of the dynamic dipole polarizability, which is a complex quantity depending on the trapping laser frequency ω and determining the optical potential depth and the photon scattering rate. We compute the dynamic dipole polarizability with a sum-over-state formula, whose versatility enables us to calculate both the real and imaginary parts of the polarizability at any desired frequency. Two theoretical values of the static ($\omega = 0$) dipole polarizability are reported in the literature [32, 33], which were calculated with purely *ab initio* methods. But as shown in recent papers, modeling lanthanides with such methods is a hard task. Here the relevant transition energies from the ground state and the related transition dipole moments are extracted from a semi-empirical approach combining quantum-chemical calculations and experimental data. One central objective of this article is to determine in which extent the non-spherical electronic distribution of erbium induces an anisotropic response to the trapping light.

Unlike alkali metals, lanthanides are characterized by a complex electronic structure since they possess an open $4f$ and/or $5d$ subshells in their electronic core, which is surrounded by a closed $6s$ shell. Since the electronic angular momentum associated with such configurations is larger, the electronic distribution of a particular Zeeman sublevel is strongly anisotropic. In addition the excitation of the core electrons occurring around 10000 cm^{-1} above the ground-state energy gives birth to very rich and complex spectra whose interpretation was an important part of atomic physics in the last decades [34, 35]. Today the knowledge of the spectroscopy of neutral and charged lanthanides including erbium is still incomplete [36–38]. Therefore using the Racah-Slater least-square fitting method implemented in the Cowan suite of codes [34], we adjust calculated and experimental energy levels. This allows us to give a new theoretical interpretation of the spectrum of neutral erbium, and to predict 9 new levels accessible from the ground state through electric-dipole transition.

Since we manipulate a lot of atomic data in this paper, it is necessary to precise how energy levels are labeled. Although an atomic level can be unambiguously defined with its energy with respect to the ground state [39], information about electronic angular momenta is also crucial. Strictly speaking, the only good quantum numbers are J the total (orbital+spin) angular momentum, M_J its projection on the quantization axis z , and p the parity. For particular states, *e.g.* the lowest states of erbium, the total orbital and spin angular momenta, L and S respectively, are almost good quantum numbers. We also use the leading electronic configuration whose weight depends on the state under consideration (see the Appendix at the end of the paper). For example, ground-state erbium is of even parity and its total angular momentum is $J = 6$. It is of 3H character ($L = 5$, $S = 1$) up to 99 %, the rest being 1I ; its leading configuration is $[\text{Xe}]4f^{12}6s^2$. Since our calculations are mostly based on the Wigner-Eckart theorem, we will often label the atomic levels as $|\beta JM_J\rangle$, where β stands for all quantum numbers except J and M_J .

The paper is organized as follows. In Section II we give all the formulas necessary to characterize the optical trapping of non-spherically-symmetric atoms, in particular the potential depth and the photon-scattering rate induced by the trapping light. Section III is dedicated to the spectroscopy of erbium. We first recall the main steps of the present approach based on the Cowan suite of codes, and we present our results for energies and transition dipole moments. In section IV we report on our tests and results for the polarizabilities of ground-state erbium. The reader interested in the final results is invited to go to subsection IV C. Finally section V contains concluding remarks, emphasizing on the van der Waals interactions between two erbium atoms. More details on the atomic structure calculations are reported in a final Appendix including tables for fitting parameters used to model the erbium spectrum, energies,

Landé factors, and configuration weights.

II. OPTICAL TRAPPING OF NON-SPHERICAL ATOMS

When spherically-symmetric atoms, like 2S alkali-metal or 1S alkaline-earth atoms, are submitted to a light wave of angular frequency ω and intensity $I(\mathbf{r})$, with \mathbf{r} the atomic center-of-mass position in the lab frame xyz , z being the quantization axis, they experience a potential energy [40]

$$U(\mathbf{r}; \omega) = -\frac{1}{2\epsilon_0 c} \Re[\alpha_{\text{scal}}(\omega)] \times I(\mathbf{r}), \quad (1)$$

which is due to the second-order ac Stark effect. In Eq. (1), $\alpha_{\text{scal}}(\omega)$ is the (complex) scalar dynamic dipole polarizability of the atom, $\Re[\dots]$ denoting the real part, ϵ_0 is the vacuum permittivity and c the speed of light. The presence of the electromagnetic field also induces photon scattering with a rate equal to [40]

$$\Gamma(\mathbf{r}; \omega) = \frac{1}{\hbar\epsilon_0 c} \Im[\alpha_{\text{scal}}(\omega)] \times I(\mathbf{r}), \quad (2)$$

where now $\Im[\alpha_{\text{scal}}(\omega)]$ is the imaginary part of the dynamic scalar dipole polarizability.

The complex polarizability is calculated by using the second-order time-dependent perturbation theory, which is cautiously discussed in Ref. [41], and by attributing to each excited level a complex energy $E_{\beta'J'} - i\hbar\gamma_{\beta'J'}/2$, $\gamma_{\beta'J'}$ being the inverse lifetime of the level [42]. This gives

$$\alpha_{\text{scal}}(\omega) = \frac{1}{3(2J+1)} \sum_{\beta'J'} \left(\frac{\langle \beta'J' \parallel d \parallel \beta J \rangle^2}{E_{\beta'J'} - E_{\beta J} - i\frac{\hbar\gamma_{\beta'J'}}{2} - \hbar\omega} + \frac{\langle \beta'J' \parallel d \parallel \beta J \rangle^2}{E_{\beta'J'} - E_{\beta J} - i\frac{\hbar\gamma_{\beta'J'}}{2} + \hbar\omega} \right) \quad (3)$$

with $\langle \beta'J' \parallel d \parallel \beta J \rangle$ the reduced transition dipole moment. Then considering that the laser frequency is far from any atomic resonance, namely $(E_{\beta'J'} - E_{\beta J} - \hbar\omega) \gg \hbar\gamma_{\beta'J'}/2$, and *a fortiori* $(E_{\beta'J'} - E_{\beta J} + \hbar\omega) \gg \hbar\gamma_{\beta'J'}/2$ since the atoms are in the ground state, we can separate real and imaginary parts

$$\Re[\alpha_{\text{scal}}(\omega)] = \frac{2}{3(2J+1)} \sum_{\beta'J'} \frac{(E_{\beta'J'} - E_{\beta J}) \langle \beta'J' \parallel d \parallel \beta J \rangle^2}{(E_{\beta'J'} - E_{\beta J})^2 - \hbar^2\omega^2} \quad (4)$$

$$\Im[\alpha_{\text{scal}}(\omega)] = \frac{1}{3(2J+1)} \sum_{\beta'J'} \frac{(E_{\beta'J'} - E_{\beta J})^2 + \hbar^2\omega^2}{[(E_{\beta'J'} - E_{\beta J})^2 - \hbar^2\omega^2]^2} \hbar\gamma_{\beta'J'} \langle \beta'J' \parallel d \parallel \beta J \rangle^2. \quad (5)$$

For non-spherically-symmetric atoms like erbium, the ac-Stark shift depends on the magnetic sublevel M_J and on the light polarization. In the general case of an elliptically-polarized light whose unit vector of polarization is \mathbf{e} , the trapping potential equals [43]

$$U_{M_J}^{\text{ell}}(\mathbf{r}; \theta_p, \theta_k, \mathcal{A}; \omega) = -\frac{1}{2\epsilon_0 c} I(\mathbf{r}) \left\{ \Re[\alpha_{\text{scal}}(\omega)] + \mathcal{A} \cos \theta_k \frac{M_J}{2J} \Re[\alpha_{\text{vect}}(\omega)] + \frac{3M_J^2 - J(J+1)}{J(2J+1)} \times \frac{3 \cos^2 \theta_p - 1}{2} \Re[\alpha_{\text{tens}}(\omega)] \right\}, \quad (6)$$

where θ_p is such that $|\mathbf{e} \cdot \mathbf{e}_z|^2 = \cos^2 \theta_p$, θ_k is the angle between z and the wave vector, and \mathcal{A} the ellipticity parameter. Similarly to Eqs. (1) and (2) the photon-scattering rate $\Gamma_{M_J}^{\text{ell}}$ is obtained by replacing $\Re[\dots]$ by $\Im[\dots]$ in Eq. (6). The quantities $\alpha_{\text{vect}}(\omega)$ and $\alpha_{\text{tens}}(\omega)$ are respectively the vector and tensor dynamic dipole polarizabilities, given by

$$\Re[\alpha_{\text{vect}}(\omega)] = 2 \sum_{\beta'J'} X_{JJ'}^{(1)} \frac{\hbar\omega \langle \beta'J' \parallel d \parallel \beta J \rangle^2}{(E_{\beta'J'} - E_{\beta J})^2 - \hbar^2\omega^2} \quad (7)$$

$$\Im[\alpha_{\text{vect}}(\omega)] = 2 \sum_{\beta'J'} X_{JJ'}^{(1)} \frac{\hbar^2\omega \gamma_{\beta'J'} (E_{\beta'J'} - E_{\beta J})}{[(E_{\beta'J'} - E_{\beta J})^2 - \hbar^2\omega^2]^2} \langle \beta'J' \parallel d \parallel \beta J \rangle^2 \quad (8)$$

$$\Re[\alpha_{\text{tens}}(\omega)] = 4 \sum_{\beta'J'} X_{JJ'}^{(2)} \frac{(E_{\beta'J'} - E_{\beta J}) \langle \beta'J' \parallel d \parallel \beta J \rangle^2}{(E_{\beta'J'} - E_{\beta J})^2 - \hbar^2\omega^2} \quad (9)$$

$$\Im[\alpha_{\text{tens}}(\omega)] = 2 \sum_{\beta'J'} X_{JJ'}^{(2)} \frac{(E_{\beta'J'} - E_{\beta J})^2 + \hbar^2\omega^2}{[(E_{\beta'J'} - E_{\beta J})^2 - \hbar^2\omega^2]^2} \hbar\gamma_{\beta'J'} \langle \beta'J' \parallel d \parallel \beta J \rangle^2, \quad (10)$$

where $X_{JJ'}^{(k)}$ are angular factors [44]

$$X_{JJ'}^{(1)} = (-1)^{J+J'} \sqrt{\frac{6J}{(J+1)(2J+1)}} \left\{ \begin{array}{ccc} 1 & 1 & 1 \\ J & J & J' \end{array} \right\} \quad (11)$$

$$X_{JJ'}^{(2)} = (-1)^{J+J'} \sqrt{\frac{5J(2J-1)}{6(J+1)(2J+1)(2J+3)}} \left\{ \begin{array}{ccc} 1 & 1 & 2 \\ J & J & J' \end{array} \right\}. \quad (12)$$

The particular case of a circular right (left) polarization is obtained by setting $\mathcal{A} = +1$ (-1) in Eq. (6). In a linearly-polarized light, corresponding to $\mathcal{A} = 0$, the trapping depends neither on the angle θ_k nor on the vector polarizability. In this case $\theta_p = \theta$ is the angle between the polarization vector \mathbf{e} and the quantization axis z . The trapping potential $U_{M_J}^{\text{lin}}$ is obtained from Eq. (6)

$$U_{M_J}^{\text{lin}}(\mathbf{r}; \theta; \omega) = U_{M_J}^{\text{ell}}(\mathbf{r}; \theta_p = \theta, \theta_k, \mathcal{A} = 0; \omega) \quad (13)$$

and similarly $\Gamma_{M_J}^{\text{lin}}(\mathbf{r}; \theta; \omega) = \Gamma_{M_J}^{\text{ell}}(\mathbf{r}; \theta_p = \theta, \theta_k, \mathcal{A} = 0; \omega)$.

III. THEORETICAL INTERPRETATION OF NEUTRAL ERBIUM SPECTRUM

Equations (4), (5) and (7)–(10) above show that the polarizabilities crucially depend on the transition energies and transition dipole moment from erbium ground state. Therefore the quality of those data as well as the method to calculate them represent a central issue of this work.

The initial steps that led to the critical compilation of erbium energy levels were summarized by Martin *et al.* in [45] and later reported in the NIST database [39]. After 1978, systematic studies of hyperfine effects in $4f^n5d6s6p$ configurations of neutral lanthanides addressed the case of neutral erbium (Er I); but the fine-structure study preceding the determination of magnetic dipole and electric quadrupole parameters had to be limited to the terms of $4f^{11}5d6s6p$ arising from the ground term 4I of the core [46].

A first step in the description of Er I levels by means of the Cowan suite of codes [34] was used in an experimental determination of transition probabilities [38]. The Cowan codes led to energies and eigenfunctions by least squares determination of radial parameters in appropriate sets of interacting electronic configurations, following the Racah-Slater method as reminded in [47]. The case of Er I turned out to be more complex than singly-ionized erbium (Er II) [36], because in neutral lanthanides the lower levels of many excited configurations overlap the upper part of low-lying configurations. Before 1976, some levels with $7s, 8s, 6d$ electrons were identified by means of very selective decays (from $4f^{12}6s(7s, 8s, 6d)$ to $4f^{12}6s6p$ and from $4f^{11}5d6s7s$ to $4f^{11}5d6s6p$ and of hazy emission line profiles that are common for such transitions in lanthanides. The semi-empirical designations were tabulated in [39, 45]. As concerns combinations of valence electrons, estimates by Brewer [48, 49] place the lowest levels of odd parity configurations $4f^{12}5d6p, 4f^{11}5d^3, 4f^{11}6s6p^2$, and $4f^{13}6s$ in the energy range $37000\text{--}43000 \text{ cm}^{-1}$ above the ground level $4f^{12}6s^2\ ^3H_6$. In the even parity, $4f^{11}5d^26p, 4f^{12}6p^2$ and $4f^{12}5d^2$ should be present above $38500 \pm 2000 \text{ cm}^{-1}$. The three unknown configurations with $4f^{11}$ core totalize 10914 predicted levels and the four others 1258 levels. The limitations imposed by available computers are less tight than in earlier studies but the applicability of the parametric fitting in the Racah-Slater method is decreased when thousands of adjustable parameters are introduced by several tens of configurations. This guided us in the choice of the electronic configurations included in the model. In the even parity, since we focus on Er I ground state, we consider the lowest configuration $4f^{12}6s^2$. In the odd parity, we added the high-lying electronic configurations $4f^{12}5d6p$ and $4f^{13}6s$ to the known low-lying ones $4f^{11}5d6s^2, 4f^{12}6s6p$ and $4f^{11}5d^26s$.

Let us briefly recall the principle of the calculations with the Cowan suite.

1. First for each configuration separately, the RCN program calculates the electronic wave functions using the relativistic Hartree-Fock (HFR) method.
2. Then RCN2 calculates various radial integrals including: for a given configuration, the direct and exchange Coulombic integrals $F^k(n\ell n'\ell')$ and $G^k(n\ell n'\ell')$ (for equivalent and non-equivalent electrons), the spin-orbit energy $\zeta_{n\ell}$ for each subshell; for each couple of configurations, the configuration-interaction Coulombic integrals $R^k(n\ell n'\ell', n''\ell'' n''' \ell'''')$. The radial integrals are treated in step (4) as adjustable parameters.
3. Using those radial integrals, RCG diagonalizes the atomic Hamiltonian in appropriate angular-momentum bases, *e.g.* given values of J . From the resulting eigenenergies and eigenvectors, it models the atomic spectrum by calculating in particular the Einstein coefficient for all possible electric-dipole transitions.

4. The energies calculated by RCG are then compared to the tabulated experimental levels. A fit on the atomic parameters is performed by the RCE code in order to minimize the mean error between experimental and theoretical energies. It produces a new set of parameters which serves as input for RCG (step (3)). Then a few RCG-RCE loops are performed to minimize the mean error.

We used both the LANL [50] and the Kramida [51] versions of Cowan codes.

The optimal atomic parameters, which make the input for the last call of RCG, are given in appendix (see Tables III and IV). In the odd parity, 208 levels of the mixed configurations $4f^{11}5d6s^2$, $4f^{11}5d^26s$, $4f^{12}6s6p$ are used to determine 24 free parameters, 88 other parameters being constrained. The mean error is 65 cm^{-1} . The results are given in the appendix (see Tables V and VI). The general agreement between experimental and theoretical Landé factors is a first indication of the quality of the eigenfunctions. The only noticeable exception is the inversion of the close $J = 5$ levels at 28026 and 28129 cm^{-1} .

IV. CALCULATION OF ERBIUM POLARIZABILITIES

A. Data sets of transition energies and dipole moments

The output of the previous calculations consists in a list of transition energies and Einstein coefficients, hence of reduced transition dipole moments, from ground-state erbium, which can be used in our sum-over-state formulas of the polarizabilities (see Eqs. (4), (5), (7–10)). We call that list the data set T (after “theoretical”).

The data set T has been optimized so that the calculated energies match as well as possible the experimental ones. To obtain better values of the polarizabilities, we apply a second step of optimization by adjusting the monoelectronic radial integrals $\langle n'\ell'|\hat{r}|n\ell \rangle$ to minimize the standard error on Einstein coefficients A_i

$$\sigma = \left(\sum_{i=1}^{N_{\text{lev}}} \frac{(A_i^{\text{th}} - A_i^{\text{exp}})^2}{N_{\text{lev}} - N_{\text{par}}} \right)^{1/2}, \quad (14)$$

where N_{lev} and N_{par} are the numbers of levels and adjusted parameters respectively. In this section we discuss in details the influence on (14) of the scaling factors

$$f_{n\ell n'\ell'} = \frac{\langle n'\ell'|\hat{r}|n\ell \rangle}{\langle n'\ell'|\hat{r}|n\ell \rangle_{\text{RHF}}} \quad (15)$$

with $\langle n'\ell'|\hat{r}|n\ell \rangle_{\text{RHF}}$ the relativistic Hartree-Fock radial integral calculated by the Cowan code RCN2.

In order to evaluate the reliability of the data set T, we also consider the 33 lines ending in ground-state erbium which were experimentally detected by Lawler and coworkers [38]; we obtain the data set E (after “experimental”). Theory and experiment can be directly compared by extracting among the lines of data set T those which have an experimental counterpart; this gives the data set T'.

B. Convergence and uncertainty

Now we discuss the convergence and reliability of our calculations, taking mostly the example of the real part of the static scalar polarizability $\Re[\alpha_{\text{scal}}(\omega = 0)]$ (see Eq. (4)). This quantity is not relevant in the context of optical trapping (except for CO₂-laser traps) but there exists two theoretical values in the literature to which our results can be compared: 153 a.u. from Ref. [33] and 166 a.u. from Ref. [32]. The conclusions drawn for $\omega = 0$ can actually be extended up to the first main resonances $\omega \lesssim 20000 \text{ cm}^{-1}$. Note that the imaginary part of the static scalar polarizability will be examined separately.

1. Influence of data sets and scaling factors.

First, the influence of the different data sets with no adjustment on the scaling factors ($f_{n\ell n'\ell'} = 1$) is addressed (see first three lines of Table I). The two theoretical values T and T' clearly exceed the experimental one E. To have better an agreement between E and T', we should use radial scaling factors smaller than unity. In addition since for zero or weak frequencies, the scalar polarizability [Eq. (4)] is a sum of positive terms, and since the set of experimental lines is *a priori* incomplete, the value from data set E (132 a.u.) can be regarded as the lower bound for $\alpha_{\text{scal}}(0)$.

TABLE I. Static scalar dipole polarizability $\Re[\alpha_{\text{scal}}(\omega = 0)]$ for the different data sets and different scaling factors f for the mono-electronic radial integrals (see text).

data set	scaling factor f	$\Re[\alpha_{\text{scal}}(0)]$
E	-	132
T'	1	200
T	1	226
T	0.81	148
T	0.77	134

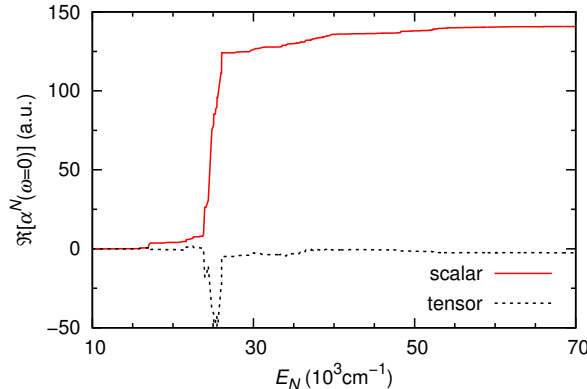


FIG. 1. (Color online) Convergence of the real part of the static scalar polarizability $\Re[\alpha_{\text{scal}}^N(\omega = 0)]$ (solid line), and the static tensor polarizability $\Re[\alpha_{\text{tens}}^N(\omega = 0)]$ (dotted line), with respect to the excited states of data set T. Eqs. (4) and (9) are truncated up to the excited state of energy E_N .

Given the configurations of odd parity that we include in our calculation of erbium spectrum (see Sec. III), the transition-dipole-moment matrix elements involve two radial integrals: $\langle 4f|\hat{r}|5d\rangle$ and $\langle 6s|\hat{r}|6p\rangle$. We calculated the standard error on Einstein coefficients (14) between sets E and T', and we found that: (i) it is much less sensitive to $f_{4f,5d}$ than to $f_{6s,6p}$; (ii) the standard error is minimum ($\sigma = 1.36 \times 10^7 \text{ s}^{-1}$ with $N_{\text{lev}} = 33$ and $N_{\text{par}} = 2$) for $f_{6s,6p} = 0.77$. The corresponding polarizability is 118 and 134 a.u. for data sets T' and T respectively. A closer look at the result shows that this scaling factor minimizes the error on the strongest line, whose upper level is the one of $J = 7$ at 24943 cm^{-1} .

We made another test by searching the factor f giving the same result for the data sets T' and E. We found $f = 0.81$ and the corresponding polarizability 148 a.u.. The two “optimal” scaling factors ($f = 0.77$ and 0.81) are rather close to each other. Their discrepancy can be explained because the second criterion allows for compensation effects between theoretical Einstein coefficient larger and smaller than the experimental ones.

In conclusion, we take the previous results as our lower and upper bonds, and we take $f = 0.79$ for our recommended value. Finally we obtain $\Re[\alpha_{\text{scal}}(\omega = 0)] = 141 \pm 7 \text{ a.u.}$, which is in a good agreement although smaller than the two literature values.

2. Convergence on excited energy levels.

Now that the question of scaling factors is solved, we discuss the convergence of the sum-over-state formulas inside the list of excited states in data set T. Namely, we truncate Eqs. (4), (5), (9) and (10) up to a given excited state $|N\rangle = |\beta_N J_N\rangle$ of energy E_N , and we plot the resulting polarizabilities $\alpha_{\text{scal}}^N(\omega = 0)$ and $\alpha_{\text{tens}}^N(\omega = 0)$ as functions of E_N (note that $\alpha_{\text{vecl}}(\omega = 0) = 0$).

On Fig. 1 we focus on the real part of the scalar and tensor polarizabilities. We see that they are converged for $E_N \approx 60000 \text{ cm}^{-1}$, where they reach at least 99 % of their total value. In addition, the scalar polarizability reaches already 90 % of its total value at $E_N \approx 30000 \text{ cm}^{-1}$, that is when the strongest lines have been included in the sum. In comparison, the lowest energies associated with configurations not included in our calculation are estimated around 40000 cm^{-1} above the ground state [48, 49]. The convergence is visible on the tensor polarizability, although less spectacular, because the angular factor $X_{JJ'}^{(2)}$ [Eq. (12)] can change sign with J' . This fast convergence is due to

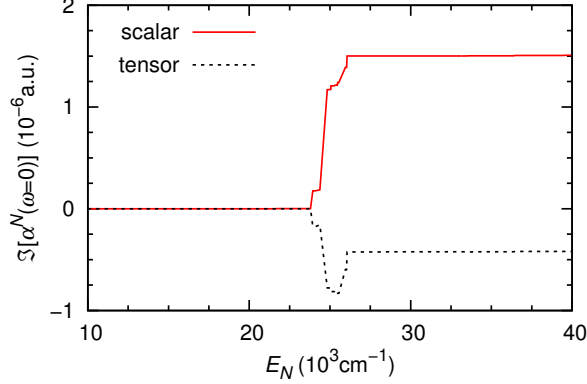


FIG. 2. (Color online) Convergence of the imaginary part of the static scalar polarizability $\Im[\alpha_{\text{scal}}^N(\omega = 0)]$ (solid line), and the static tensor polarizability $\Im[\alpha_{\text{tens}}^N(\omega = 0)]$ (dashed line), with respect to the excited states of data set T. Eqs. (5) and (10) are truncated up to the excited state of energy E_N .

the $(E_{\beta'J'} - E_{\beta J})^{-1}$ factor in Eq. (7) which enhances the importance of low-energy transitions; it is also inherent to the erbium spectrum which is composed of a few strong lines among a forest of weak lines.

3. Imaginary part of the static scalar polarizability.

In order to calculate the imaginary part of the polarizabilities, we need, in addition to transition energies and transition dipole moments, the lifetimes of all the excited states. For a given state this would require to know the Einstein coefficient of all the downward transitions from this state. Here we will rather make the assumption that all the excited states can only decay to the ground state. The inverse lifetime of the state $|\beta'J'\rangle$ is then the Einstein coefficient of the transition to the ground state

$$\gamma_{\beta'J'} = \frac{E_{\beta'J'}^3 \langle \beta'J' | d | {}^3H_6 \rangle^2}{3(2J' + 1)\pi\epsilon_0\hbar^4c^3} \quad (16)$$

where we have set the ground-state to zero. We can check this hypothesis by calculating the imaginary part of the static polarizabilities with the data set E. On the one hand we use Eq. (16) and on the other hand we used the lifetimes measured by the same group [37]. We obtain a very good agreement between the two methods which respectively give $\Im[\alpha_{\text{scal}}(0)] = 1.42 \cdot 10^{-6}$ a.u., $\Im[\alpha_{\text{tens}}(0)] = -3.33 \cdot 10^{-7}$ a.u. (note that $\Im[\alpha_{\text{vect}}(0)] = 0$). Indeed Eq. (16) is a very good approximation for the lowest excited states, which are prevailing due to the $E_{\beta'J'}^{-2}$ dependence of Eqs. (5), (8) and (10).

Figure 2 shows the imaginary part of the static polarizabilities as a function of E_N . For the sake of coherence we have used the same scaling factor $f = 0.79$ as for the real part of the polarizabilities. The convergence with E_N is even faster than for the real part: at $E_N = 30000 \text{ cm}^{-1}$, $\Im[\alpha_{\text{scal}}^N(0)]$ and $\Im[\alpha_{\text{tens}}^N(0)]$ differ by less than 1 % from their final values given in Table II.

C. Results

In order to present our results in a convenient way for experimental purposes, we give the polarizabilities of erbium in atomic units (units of a_0^3 , with a_0 the Bohr radius), but also the corresponding relevant quantities in physical units. To the real part of the polarizability corresponds the trapping potential in temperature units

$$U(\text{in K}) = \frac{2\pi a_0^3}{k_B c} \Re[\alpha(\text{in a.u.})] \times I(\text{in W.m}^{-2}), \quad (17)$$

and to the imaginary part of the polarizability corresponds the photon-scattering rate

$$\Gamma(\text{in s}^{-1}) = \frac{4\pi a_0^3}{\hbar c} \Im[\alpha(\text{in a.u.})] \times I(\text{in W.m}^{-2}). \quad (18)$$

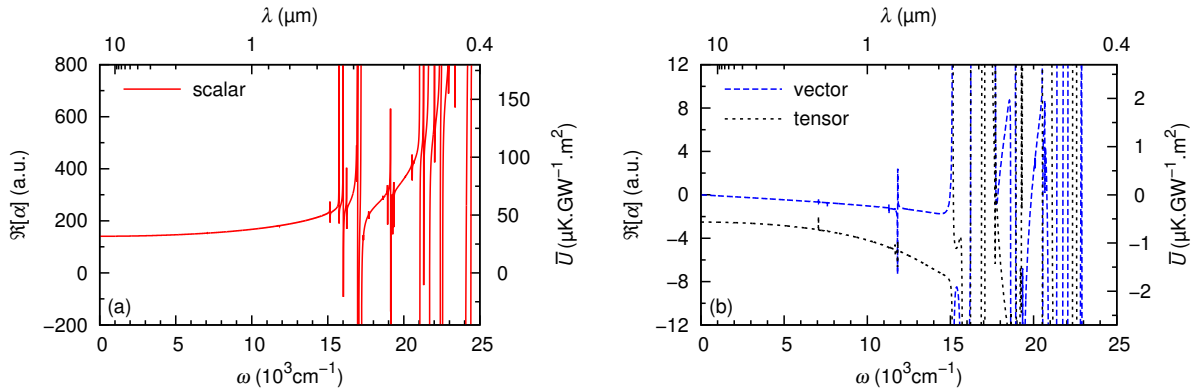


FIG. 3. (Color online) Real part of the scalar (panel a), vector and tensor (panel b, resp. dashed and dotted lines) polarizabilities in atomic units and corresponding trapping potentials obtained for an intensity of 1 GW.m^{-2} , as functions of the trapping frequency ω (or wavelength λ).

TABLE II. Real and imaginary parts of the scalar, vector and tensor polarizabilities in atomic units, at $\omega = 0$ and 9398 cm^{-1} ($\lambda = 1064 \text{ nm}$), compared with available literature values.

$\omega (\text{cm}^{-1})$	0	9398
$\Re[\alpha_{\text{scal}}]$	141	164
	153 [33]	-
	166 [32]	-
$\Re[\alpha_{\text{vect}}]$	0	-0.943
$\Re[\alpha_{\text{tens}}]$	-2.52	-3.93
	-2.73 [32]	-
$\Im[\alpha_{\text{scal}}]$	$1.51 \cdot 10^{-6}$	$2.34 \cdot 10^{-6}$
$\Im[\alpha_{\text{vect}}]$	0	$-1.74 \cdot 10^{-6}$
$\Im[\alpha_{\text{tens}}]$	$-4.21 \cdot 10^{-7}$	$-6.90 \cdot 10^{-7}$

In what follows we assume the typical intensity of 1 GW.m^{-2} (obtained for a laser power of 15 W and a gaussian beam waist of $100 \mu\text{m}$), which gives the potential $\bar{U}(\text{in } \mu\text{K.GW}^{-1} \cdot \text{m}^2) = 0.22494655 \times \Re[\alpha(\text{in a.u.})]$ and the rate $\bar{\Gamma}(\text{in } \text{s}^{-1} \cdot \text{GW}^{-1} \cdot \text{m}^2) = 5.8900155 \cdot 10^4 \times \Im[\alpha(\text{in a.u.})]$.

On Fig. 3 we plot the real part of the erbium polarizabilities and the corresponding trapping potentials as functions of the laser frequency (in cm^{-1}) and wavelength (in nm). We see a dense pattern of resonances for $\omega \geq 11000 \text{ cm}^{-1}$. But most of them are narrow, which corresponds to weak transitions from the ground state, and the background profile of the polarizabilities is inherited from the strong lines. In Tab. II we focus on two frequencies: $\omega = 0$, to compare our results to the literature; and $\omega = 9398 \text{ cm}^{-1}$ ($\lambda = 1064 \text{ nm}$) a widespread laser-trapping frequency which is in the case of erbium far from any resonance. Our scalar and tensor polarizabilities are in good agreement with Refs. [32, 33] which were calculated with different methods.

But the most striking feature is that the vector and tensor contributions are found extremely small compared to the scalar contribution. It means that the trapping potential exerted on erbium atoms is almost isotropic, in a sense that it does not depend on the respective orientation of the electronic cloud and the light polarization. One possible explanation to that phenomenon is the following: the anisotropic response to the trapping light should be due to the electrons of the unfilled $4f$ shell; but the latter is so contracted that the anisotropy is by far dominated by the isotropic response of the outermost $6s$ electrons.

The situation is drastically different for the imaginary part, for which the scalar, vector and tensor polarizabilities are of the same order of magnitude (see Fig. 4 and Tab. II). The corresponding scaled photon-scattering rates are $\sim 0.1 \text{ s}^{-1} \cdot \text{GW}^{-1} \cdot \text{m}^2$. After a cycle of absorption and spontaneous emission, a fraction of the atoms are too hot to be kept in the trap. Therefore the atomic lifetime in the trap will strongly depend on the orientation between the electronic and the light polarization. This is illustrated on Figure 5 where the reduced photon-scattering rate $\bar{\Gamma}_{-J}^{\text{lin}}$ for the lowest Zeeman sublevel is plotted as a function of the angle θ between the linearly-polarized electric field and the quantization axis (given by an external magnetic field). Due to the negative sign of $\Im[\alpha_{\text{tens}}]$ the rate is the smallest, and so the trap is the most stable, in the colinear configuration ($\theta = 0$ or 180°). A similar behavior is observed as a

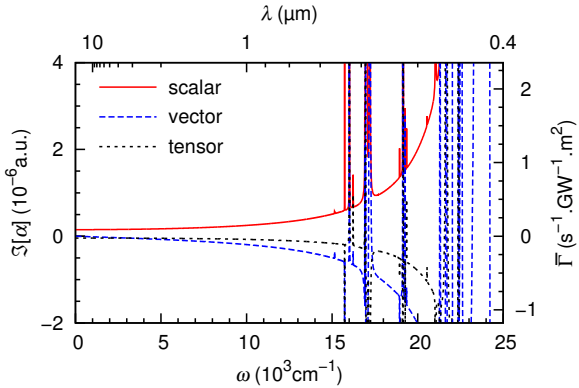


FIG. 4. (Color online) Imaginary part of the scalar, vector and tensor polarizabilities (resp. solid, dashed and dotted lines) in atomic units and corresponding photon-scattering rates obtained for an intensity of 1 GW.m^{-2} , as functions of the trapping frequency ω (or wavelength λ).

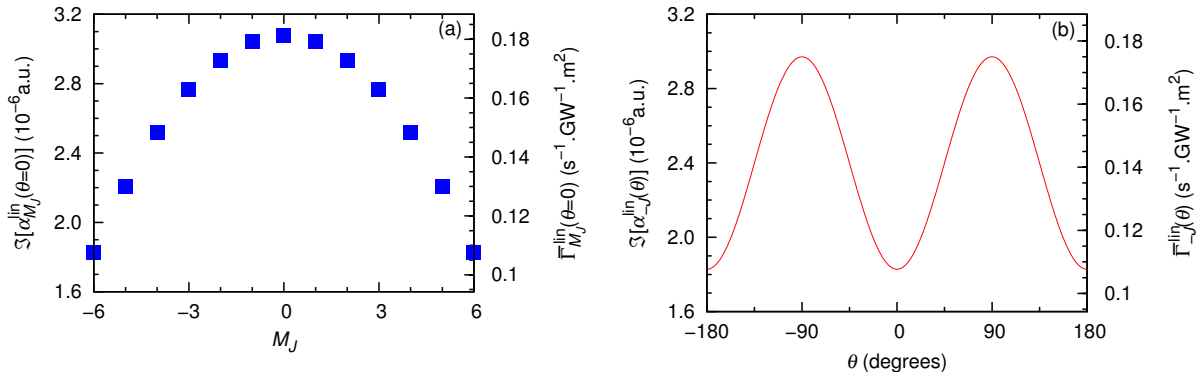


FIG. 5. (Color online) Imaginary part of the polarizability in atomic units and corresponding photon-scattering rates obtained for a 1-GW.m^{-2} linearly-polarized 1064-nm trapping light (see Eq. (2)). Panel (a) corresponds to a polarization axis parallel to the quantization axis ($\theta = 0^\circ$) and is as function of the Zeeman sublevel M_J ; while panel (b) is for the lowest sublevel $M_J = -J$ and as a function of θ .

function of M_J for a fixed angle $\theta = 0^\circ$.

V. CONCLUDING REMARKS

In this article we give a new theoretical interpretation of the spectrum of neutral erbium, which enables us to characterize the optical trapping of ultracold erbium atoms. We find 9 unobserved levels which are accessible from the ground state through electric-dipole transition. We obtain a list of transition energies and transition dipole moments that we use to calculate the real and imaginary parts of the scalar, vector and tensor contributions to the ground-state polarizability. Although erbium is a non-spherically-symmetric atom, we show that the trapping potential exerted by an infrared laser is essentially isotropic, in the sense that it depends neither on the light polarization nor on the atomic Zeeman sublevel. In contrast, the photon-scattering rate exhibits an anisotropic behavior, since the vector and tensor contributions to the imaginary part of the polarizability are of the same order of magnitude as the scalar contribution. Calculations made with different transition energy and dipole moments including experimental ones show the same trends. Ongoing experiments in the Innsbruck group should allow us to check those results.

The anisotropy of the photon-scattering rate opens the possibility to control the heating or the losses in the trap with an appropriate light polarization. The dependence of the photon-scattering rate on the atomic sublevel also results in different trap lifetimes for different Feshbach-molecular states of Er_2 which are a current subject of interest.

Our calculations of polarizabilities are also relevant to characterize the long-range interactions between two erbium atoms. For non polarized atoms, *i.e.* not in a given Zeeman sublevel, the isotropic van der Waals coefficient C_6^{iso} can be

calculated using the London formula $C_6^{\text{iso}} = -(3/\pi) \int_0^{+\infty} d\omega \Re[\alpha_{\text{scal}}(i\omega)]^2$, where $\alpha_{\text{scal}}(i\omega)$ is the scalar polarizability at imaginary frequency, which gives for ground-state erbium $C_6^{\text{iso}} = 1760$ a.u.. In the case of polarized atoms, the C_6 coefficients also have an anisotropic contribution, which is very weak compared to the isotropic one, since it is proportional to $\int_0^{+\infty} d\omega \Re[\alpha_{\text{scal}}(i\omega)]\Re[\alpha_{\text{tens}}(i\omega)] = -16.6$ a.u. and $\int_0^{+\infty} d\omega \Re[\alpha_{\text{tens}}(i\omega)]^2 = 0.265$ a.u.. The C_6 coefficients between two polarized 3H_6 erbium atoms thus range from 1741 to 1766 a.u., and show a similar variation to dysprosium atoms [52].

The knowledge of the polarizabilities of excited states, and in particular of so-called “magic” frequencies or wavelengths, *i.e.* the wavelengths for which polarizabilities of the ground state and of a given excited state are equal, is of strong importance for precision measurements [53–55]. In Ref. [25], the authors calculate magic wavelengths for dysprosium atoms in a non-polarized light. In the case of a polarized light, our preliminary calculations show that the anisotropy of trapping potential for erbium excited states tends to be larger than for the ground state. For example, at $\lambda = 1064$ nm the polarizabilities of the level $J = 7$ at 15847 cm^{-1} are $\Re[\alpha_{\text{scal}}] \approx 130$ a.u. and $\Re[\alpha_{\text{scal}}] \approx -60$ a.u.. So for the $M_J = -7$ sublevel in a linearly-polarized electric field, $\Re[\alpha_{M_J=-7}]$ varies from 70 a.u. for $\theta = 0^\circ$ to 160 a.u. for $\theta = 90^\circ$ [see Eq. (13)]. This opens the possibility of a better control of the trapping conditions, by tuning both the laser wavelength and the polarization angle, as recently shown for diatomic molecules [56].

ACKNOWLEDGMENTS

Enlightening discussions with the members of the experimental team of Francesca Ferlaino in Innsbruck, in particular Kiyotaka Aikawa, Simon Baier, Albert Frisch and Michael Mark, are gratefully acknowledged. ML is grateful to Eliane Luc for her guidance in theory of atomic structure. JFW acknowledges Laboratoire Aimé Cotton for its hospitality. Laboratoire Aimé Cotton is a member of *Institut Francilien de Recherche sur les Atomes Froids* (www.ifraf.org).

Appendix A: Details of the atomic-structure calculations

This appendix gives details on the calculation of the erbium atomic spectrum. Tables III and IV contains the optimal set of atomic parameters used for the last call of the diagonalization program RCG. For a given atomic parameter P , we multiply the HFR value by a scaling factor $SF(P)$, to obtain the input for the first call of RCG. The scaling factors $SF(P)$ given in Table III and IV were taken from our previous work on Er II [36]. In addition to E_{av} , $F^k(n\ell n\ell')$, $G^k(n\ell n\ell')$, $\zeta_{n\ell}$ and $R^k(n\ell n'\ell', n''\ell''n'''\ell''')$, the presence of effective parameters for accounting CI second order effects of far configurations. As explained in [34, 35], those parameters are α , β and γ for the configurations $4f^{11}$ and $4f^{12}$ and Slater-forbidden parameters $F^1(4f, 5d)$, $G^2(4f, 5d)$ and $G^4(4f, 5d)$ for the configurations with open $4f$ and $5d$ subshells. Due to the lack of HFR evaluations, initial values for effective parameters are derived from semi-empirical comparisons with similar spectra. Finally Tables V and VI contain the characteristics of the calculated even- and odd-parity levels of Er I respectively.

TABLE III: Fitted one-configuration parameters (in cm^{-1}) for odd-parity configurations of Er I compared with HFR radial integrals. The scaling factors are $SF(P) = P_{\text{fit}}/P_{\text{HFR}}$, except for E_{av} when they are $P_{\text{fit}} - P_{\text{HFR}}$. The HFR values of E_{av} parameters are relative to the ground state configuration $4f^{12}6s^2$ taken as zero value. Some parameters are constrained to vary in a constant ratio r_n , indicated in the second column except if ‘fix’ appears in the second or in the uncertainty columns. In this case, the parameter P is not adjusted.

Param.	P	$4f^{11}5d6s^2$				$4f^{11}5d^26s$				
		Cons.	P_{fit}	Unc.	P_{HFR}	SF	P_{fit}	Unc.	P_{HFR}	
E_{av}			46389	68	6742	39647	65582	74	23334	42248
$F^2(4f4f)$	r_1	97984	387	128939	0.760	97812	387	128712	0.760	
$F^4(4f4f)$	r_2	69490	308	80847	0.860	69360	307	80696	0.860	
$F^6(4f4f)$	r_3	49446	631	58150	0.850	49351	630	58039	0.850	
α	r_4	21.0	2			21.0	2			
β	fix	-650				-650				
γ	fix	2000				2000				
$F^2(5d5d)$						21541	323	32674	0.659	
$F^4(5d5d)$						16590	611	20683	0.802	
ζ_{4f}	r_5	2381	4	2428	0.981	2379	4	2426	0.981	
ζ_{5d}	r_6	803	9	948	0.847	665	7	785	0.847	

TABLE III: Fitted parameters in Er I (continued)

Param.	P	Cons.	Fitted parameters				Fitted parameters			
			P_{fit}	Unc.	P_{HFR}	SF	P_{fit}	Unc.	P_{HFR}	SF
$F^1(4f5d)$		r_7	671	70			671	70		
$F^2(4f5d)$		r_8	15594	246	20265	0.770	13496	213	17539	0.769
$F^4(4f5d)$		r_9	10737	353	9189	1.168	9123	300	7807	1.169
$G^1(4f5d)$		r_{10}	4997	121	8711	0.574	4277	104	7456	0.574
$G^2(4f5d)$		r_{11}	1238	291			1238	291		
$G^3(4f5d)$		r_{12}	6103	286	6893	0.885	5170	242	5840	0.885
$G^4(4f5d)$		r_{13}	1353	470			1353	470		
$G^5(4f5d)$		r_{14}	4034	278	5204	0.775	3406	235	4394	0.775
$G^3(4f6s)$		r_{15}					1080	90	1486	0.727
$G^2(5d6s)$		r_{17}					12159	246	19202	0.633
<hr/>										
<hr/>										
<hr/>										
<hr/>										
<hr/>										
<hr/>										
<hr/>										
<hr/>										
<hr/>										
<hr/>										
<hr/>										
<hr/>										
<hr/>										
<hr/>										
<hr/>										
<hr/>										
<hr/>										
<hr/>										
<hr/>										
<hr/>										
<hr/>										
<hr/>										
<hr/>										
<hr/>										
<hr/>										
<hr/>										
<hr/>										
<hr/>										
<hr/>										
<hr/>										
<hr/>										
<hr/>										
<hr/>										
<hr/>										
<hr/>										
<hr/>										
<hr/>										
<hr/>										
<hr/>										
<hr/>										
<hr/>										
<hr/>										
<hr/>										
<hr/>										
<hr/>										
<hr/>										
<hr/>										
<hr/>										
<hr/>										
<hr/>										
<hr/>										
<hr/>										
<hr/>										
<hr/>										
<hr/>										
<hr/>										
<hr/>										
<hr/>										
<hr/>										
<hr/>										
<hr/>										
<hr/>										
<hr/>										
<hr/>										
<hr/>										
<hr/>										
<hr/>										
<hr/>										
<hr/>										
<hr/>										
<hr/>										
<hr/>										
<hr/>										
<hr/>										
<hr/>										
<hr/>										
<hr/>										
<hr/>										
<hr/>										
<hr/>										
<hr/>										
<hr/>										
<hr/>										
<hr/>										
<hr/>										
<hr/>										
<hr/>										
<hr/>										
<hr/>										
<hr/>										

TABLE IV: Fitted parameters in Er I (continued)

Param.	P	Cons.	P_{fit}	Unc.	P_{HFR}	SF
	$R^1(5d6s, 4f6p)$	fix	-2966		-5932	0.5
	$R^3(5d6s, 4f6p)$	fix	-660		-1320	0.5

TABLE V: Comparison of energies E and Landé factors g_L of Er I even-parity levels. The superscript "exp" stands for experimental values which are taken from [45]. The superscript "th" stands for the theoretical values from the present parametric calculations. Note that $\Delta E = E^{\text{exp}} - E^{\text{th}}$.

Configuration	Term	J	E^{exp}	g_L^{exp}	ΔE	g_L^{th}
$4f^{12}6s^2$	3H	6	0	1.16381	-9	1.166
$4f^{12}6s^2$	3F	4	5035.193	1.147	49	1.141
$4f^{12}6s^2$	3H	5	6958.329	1.031	-15	1.033
$4f^{12}6s^2$	3H	4	10750.982	0.936	-116	0.945
$4f^{12}6s^2$	3F	3	12377.534	1.065	-53	1.084
$4f^{12}6s^2$	3F	2	13097.906	0.750	25	0.739

TABLE VI: Same as V for Er I odd-parity levels with electric dipole decay to the ground level. The theoretical values E^{th} , the factors g_L^{th} and the percentage of calculated configurations are derived by means of the RCG code with the parameter set reported in Table III. In the configuration notations, A stands for $4f^{12}$, B for $4f^{11}$, ds^2 for $5d6s^2$, sp for $6s6p$, d^2s for $5d^26s$ and dp for $5d6p$. The lower-case letters or Arabic numbers appearing in the seventh column correspond to different intermediate coupling schemes [34].

E^{exp} [45]	E^{th}	ΔE	g_L^{exp}	g_L^{th}	Leading % leading		Configuration weight (%)					
					electr.	LS-coupling	config.	component	$B - ds^2$	$B - d^2s$	$A - sp$	$A - dp$
$J = 5$												
11401.197	11419.6	-18	1.205	1.210	$B - ds^2$	51	$B - ds^2$	$(^4I)^5G$	97.5	2.3	0.3	0
15185.352	15258.6	-7	1.160	1.170	$B - ds^2$	55	$B - ds^2$	$(^4I)^3G$	96.7	2.3	1.0	0
17029.058	17023.5	6	1.150	1.136	$B - ds^2$	37	$B - ds^2$	$(^4I)^5H$	97.3	2.3	0.3	0
17347.860	17314.6	33	1.175	1.177	$A - sp$	33	$A - sp$	$(^3H)^3Ga$	0.3	1.2	98.1	0.4
19201.343	19250.1	-49	1.060	1.059	$A - sp$	25	$A - sp$	$(^3H)^1H$	16.2	0.9	82.6	0.3
19563.116	19383.6	180	0.990	0.990	$B - ds^2$	26	$B - ds^2$	$(^4I)^5I$	81.1	2.1	16.8	0.1
20917.276	20790.1	127	0.980	0.980	$B - ds^2$	23	$B - ds^2$	$(^4I)^5K$	97.6	2.2	0.2	0
21392.817	21419.2	-26	1.005	1.019	$B - ds^2$	18	$B - ds^2$	$(^4I)^3I$	95.6	2.6	1.7	0.1
22124.268	22136.3	-12	1.285	1.264	$A - sp$	28	$A - sp$	$(^3F)^5F$	0.3	15.6	83.7	0.4
22450.111	22571.5	-121	1.360	1.370	$B - d^2s$	35	$B - d^2s$	$(^4I)^7F$	1.4	82.7	15.8	0.1
22672.766	22651.3	21	1.040	1.040	$B - ds^2$	22	$B - ds^2$	$(^4I)^5K$	92.0	3.7	4.0	0.2
23447.079	23475.0	-28	1.080	1.084	$A - sp$	23	$A - sp$	$(^3H)^5I$	1.0	1.9	96.8	0.4
23855.654	23878.9	-23	1.140	1.178	$A - sp$	26	$A - sp$	$(^3F)^5F$	1.7	1.9	96.0	0.4
23885.406	23903.7	-18	1.100	1.058	$A - sp$	22	$A - sp$	$(^3H)^5I$	4.6	1.7	93.3	0.5
24083.166	24055.6	28	1.128	1.132	$A - sp$	46	$A - sp$	$(^3H)^3Gb$	37.1	1.7	58.5	2.6
25162.553	25170.9	-8	1.010	1.016	$B - ds^2$	24	$B - ds^2$	$(^4I)^3I$	74.9	3.5	20.5	1.1
25364.012	25382.3	-18	1.180	1.183	$B - d^2s$	13	$B - d^2s$	$(^4I)^7Ha$	1.6	96.8	1.4	3.2
25681.933	25598.0	84	1.175	1.142	$B - ds^2$	20	$B - ds^2$	$(^4F)^5F$	81.1	3.0	15.0	0.9
26198.837	26145.5	53	1.045	1.069	$A - sp$	48	$A - sp$	$(^3H)^5H$	0.1	1.4	98.1	0.3
	27651.7				$B - d^2s$	41	$B - d^2s$	$(^4I)^5Fb$	2.2	97.0	0.8	0.1
27856.436	27825.9	31	1.095	1.145	$B - d^2s$	15	$B - d^2s$	$(^4I)^7G$	8.0	87.7	4.1	0.2
28026.045	28090.7	-65	1.120	1.056	$A - sp$	18	$A - sp$	$(^3H)^5I$	12.7	9.4	77.5	0.4
28129.803	28141.9	-12	1.040	1.125	$B - ds^2$	10	$B - ds^2$	$(^4G)^5G$	67.6	8.6	23.6	0.3
29272.207	29237.0	35	1.115	1.123	$B - ds^2$	37	$B - ds^2$	$(^4F)^5H$	95.1	2.7	2.1	0.1
29550.807	29770.5	-220	1.150	1.168	$B - ds^2$	32	$B - ds^2$	$(^4F)^5G$	69.7	4.6	25.0	0.7
29794.862	29821.6	-27	1.100	1.131	$A - sp$	14	$A - sp$	$(^3F)^5F$	17.1	4.5	78.1	0.3
29894.203	30064.0	-170	1.195	1.126	$B - d^2s$	17	$B - d^2s$	$(^4I)^7Ia$	1.8	90.5	7.3	0.4
30380.282	30326.8	53	1.116		$A - sp$	20	$A - sp$	$(^3F)^3Gb$	15.6	27.3	53.9	3.3
30600.160	30768.9	-169	1.195	1.093	$B - d^2s$	8	$B - d^2s$	$(^4I)^5Hc$	4.9	78.4	15.2	1.4

TABLE VI: Odd parity levels of Er I (continued)

E^{exp} [45]	E^{th}	ΔE	g_L^{exp}	g_L^{th}	Leading % leading			Configuration			
					electr. config.	LS-coupling component	$B - ds^2$	$B - d^2s$	$A - sp$	$A - dp$	
31105.090	30988.2	117	1.200	1.250	$B - ds^2$	37	$B - d^2s$ (4I) 5Fa	0.6	96.4	2.1	0.9
31194.235	31185.2	9	1.135	1.128	$B - ds^2$	16	$B - ds^2$ (4F) 5H	86.5	9.5	3.8	0.2
31364.719	31360.7	4	1.235	1.232	$A - sp$	4	$A - sp$ (3F) 5G	2.5	5.1	92.1	0.4
31442.927	31475.4	-33	1.195	1.132	$B - d^2s$	12	$B - d^2s$ (4I) 5Fa	3.7	90.5	5.2	0.6
$J = 6$											
7176.503	7185.5	-9	1.302	1.304	$B - ds^2$	77	$B - ds^2$ (4I) 5G	98.2	1.8	0	0
11799.778	11788.5	11	1.190	1.195	$B - ds^2$	39	$B - ds^2$ (4I) 5H	96.9	2.5	0.5	0
16070.095	16125.4	-55	1.200	1.169	$B - ds^2$	42	$B - ds^2$ (4I) 3H	76.5	2.3	19.1	0.2
16321.110	16347.4	-26	1.220	1.254	$A - sp$	59	$A - sp$ (3H) 5G	14.6	1.4	83.7	0.3
17073.800	17063.7	10	1.070	1.069	$A - sp$	27	$A - sp$ (3H) 3Ia	2.9	1.1	95.6	0.4
17456.383	17461.9	-6	1.070	1.058	$B - ds^2$	23	$B - ds^2$ (4I) 5I	96.5	2.7	0.8	0
19326.598	19273.3	53	1.180	1.175	$A - sp$	31	$A - sp$ (3H) 5H	0.5	0.8	98.3	0.3
19508.432	19461.5	47	0.960	0.960	$B - ds^2$	35	$B - ds^2$ (4I) 5K	96.7	2.5	0.8	0
20166.130	20213.2	-47	1.485	1.475	$B - d^2s$	78	$B - d^2s$ (4I) 7F	0.1	99.9	0	0
20737.723	20659.6	78	0.855	0.853	$B - ds^2$	49	$B - ds^2$ (4I) 5L	97.6	2.3	0.2	0
21701.885	21786.2	-84	1.055	1.045	$B - ds^2$	25	$B - ds^2$ (4I) 3I	91.3	2.9	5.5	0.2
22583.504	22501.1	82	1.130	1.137	$B - ds^2$	36	$B - ds^2$ (4F) 5G	95.6	2.5	1.8	0.1
23311.577	23311.6	0	1.250	1.267	$B - d^2s$	22	$B - d^2s$ (4I) 7Ha	0.4	97.3	2.3	0.1
23831.359	23820.4	11	1.250	1.248	$A - sp$	56	$A - sp$ (3F) 5G	0.3	2.9	96.4	0.4
24246.146	24215.8	30	1.085	1.098	$A - sp$	43	$A - sp$ (3H) 5I	1.3	1.6	96.7	0.4
24457.139	24492.3	-35	1.050	1.054	$B - ds^2$	24	$B - ds^2$ (4F) 3H	84.4	2.7	12.3	0.6
25268.259	25308.9	-40	1.185	1.166	$B - d^2s$	17	$B - d^2s$ (4I) 7G	6.3	91.8	1.7	0.1
25392.779	25419.3	-27	1.075	1.072	$B - ds^2$	21	$B - ds^2$ (4F) 5G	82.9	9.3	7.4	0.4
25880.274	26070.5	-190	1.150	1.156	$A - sp$	41	$A - sp$ (3H) 3Hb	19.9	2.3	75.7	2.1
26237.004	26178.0	59	1.160	1.158	$A - sp$	36	$A - sp$ (3H) 3Ha	15.3	2.7	80.1	1.9
27582.017	27490.5	91	1.120	1.113	$B - d^2s$	12	$B - d^2s$ (4I) 5Ha	0.5	98.9	0.4	0.2
27879.416	27996.0	-117	1.175	1.147	$B - ds^2$	23	$B - ds^2$ (4G) 5G	90.0	7.9	2.0	0.1
28854.941	28902.8	-48	1.190	1.208	$B - d^2s$	22	$B - d^2s$ (4I) 5Gb	3.1	96.0	0.8	0.1
29152.796	29118.8	34	1.175	1.192	$B - d^2s$	15	$B - d^2s$ (4I) 7Hb	0.6	99.0	0.1	0.2
29561.425	29584.5	-24	1.130	1.126	$A - sp$	25	$A - sp$ (3F) 5G	0.2	3.1	96.2	0.4
	29718.1				$B - d^2s$	9	$B - d^2s$ (4I) 3Ic	16.1	81.3	2.3	0.3
30007.369	30051.0	-44	1.090	1.092	$B - ds^2$	14	$B - ds^2$ (2H) 1I2	67.8	31.2	0.9	0.1
30088.200	30169.1	-81	1.120	1.126	$B - d^2s$	17	$B - d^2s$ (4I) 7Ka	12.1	87.3	0.4	0.2
	30702.6				$B - d^2s$	26	$B - d^2s$ (4I) 5Ga	1.6	97.6	0.3	0.4
30765.720	30771.7	-6	1.205	1.205	$B - ds^2$	51	$B - ds^2$ (4F) 5H	95.6	4.4	0.1	0
31205.223	31264.5	-59	1.100	1.090	$B - d^2s$	14	$B - d^2s$ (4I) 7Ia	0.6	99.1	0.1	0.2
31823.748	31706.0	118	1.045	1.078	$A - sp$	39	$A - sp$ (3H) 3Ib	6.7	27.7	61.9	3.7
31926.003	31939.5	-13	1.215	1.215	$B - d^2s$	18	$B - d^2s$ (4I) 5Gd	4.1	76.4	18.0	1.5
$J = 7$											
7696.956	7713.9	-17	1.266	1.262	$B - ds^2$	78	$B - ds^2$ (4I) 5H	98.0	2.0	0	0
11887.503	11937.5	-50	1.153	1.150	$B - ds^2$	47	$B - ds^2$ (4I) 3I	96.6	2.9	0.5	0
15846.549	15844.1	2	1.070	1.066	$B - ds^2$	43	$B - ds^2$ (4I) 5K	96.6	2.4	0.9	0
17157.307	17129.3	28	1.195	1.192	$A - sp$	39	$A - sp$ (3H) 5I	1.9	1.1	96.6	0.4
17796.139	17809.4	-13	1.110	1.107	$B - ds^2$	48	$B - ds^2$ (4I) 5I	95.4	2.8	1.7	0.0
18774.123	18737.9	36	0.965	0.967	$B - ds^2$	45	$B - ds^2$ (4I) 5L	97.6	2.4	0	0
19125.253	19052.2	73	1.235	1.244	$A - sp$	68	$A - sp$ (3H) 5H	0	1.0	98.6	0.4
21168.430	21162.2	6	1.065	1.062	$B - ds^2$	33	$B - ds^2$ (4I) 3K	95.9	2.9	1.1	0.1
21787.932	21749.2	39	1.350	1.360	$B - d^2s$	49	$B - d^2s$ (4I) 7G	0.2	99.8	0	0
23080.952	23046.6	34	1.010	1.011	$B - ds^2$	40	$B - ds^2$ (4I) 3L	97.0	2.8	0.2	0
23364.853	23396.3	-31	1.225	1.226	$B - d^2s$	24	$B - d^2s$ (4I) 7G	0.3	99.6	0.2	0
24943.272	24946.1	-3	1.160	1.145	$A - sp$	57	$A - sp$ (3H) 3Ib	3.9	6.5	84.6	4.9
25159.143	25167.9	-9	1.170	1.170	$B - d^2s$	12	$B - d^2s$ (4I) 7Ha	0.9	93.8	4.9	0.4
25598.286	25570.2	28	1.155	1.166	$A - sp$	48	$A - sp$ (3H) 5I	0.4	2.0	97.1	0.5
	25659.2				$B - ds^2$	48	$B - ds^2$ (4F) 5H	96.6	3.1	0.3	0
27230.646	27134.8	96	1.135	1.113	$B - d^2s$	12	$B - d^2s$ (4I) 1Ka	0.2	99.5	0.1	0.2
27306.747	27432.5	-126	1.225	1.243	$B - d^2s$	25	$B - d^2s$ (4I) 7Hb	0.1	99.8	0	0.1
28017.584	28087.3	-70	1.080	1.068	$B - ds^2$	24	$B - ds^2$ (2H) 3K2	93.5	6.5	0	0
	28306.8				$B - d^2s$	19	$B - d^2s$ (4I) 7Hb	1.8	98.0	0.1	0.1

TABLE VI: Odd parity levels of Er I (continued)

E^{exp} [45]	E^{th}	ΔE	g_L^{exp}	g_L^{th}	Leading % leading		Configuration				
					electr.	LS-coupling	weight (%)	$B - ds^2$	$B - d^2s$	$A - sp$	$A - dp$
29088.0		1.171	$B - d^2s$	18	$B - d^2s$	$(^4I)^5Hb$	2.1	97.9	0	0	
29781.0		1.069	$B - d^2s$	15	$B - d^2s$	$(^4I)^1Kb$	1.8	98.0	0	0.2	
30127.6		1.215	$B - d^2s$	21	$B - d^2s$	$(^4I)^5Hf$	12.0	87.9	0.1	0.1	
30353.5		1.117	$B - d^2s$	17	$B - ds^2$	$(^2H)^3I2$	45.1	54.6	0.2	0.1	

REFERENCES

- [1] L. D. Carr and J. Ye. Focus on cold and ultracold molecules. *New J. Phys.*, 11(5):055009, 2009.
- [2] O. Dulieu and C. Gabbanini. Formation and interactions of cold and ultracold molecules : new challenges for interdisciplinary physics. *Rep. Prog. Phys.*, 72(8):086401, 2009.
- [3] M.A. Baranov. Theoretical progress in many-body physics with ultracold dipolar gases. *Phys. Rep.*, 464(3):71–111, 2008.
- [4] T. Lahaye, C. Menotti, L. Santos, M. Lewenstein, and T. Pfau. The physics of dipolar bosonic quantum gases. *Rep. Prog. Phys.*, 72(12):126401, 2009.
- [5] I. Bloch, J. Dalibard, and S. Nascimbène. Quantum simulations with ultracold quantum gases. *Nature Phys.*, 8(4):267–276, 2012.
- [6] V. Galitski and I. B. Spielman. Spinorbit coupling in quantum gases. *Nature*, 494(7435):49–54, 2013.
- [7] D. Wang, J. Qi, M.F. Stone, O. Nikolayeva, H. Wang, B. Hattaway, S.D. Gensemer, P.L. Gould, E.E. Eyler, and W.C. Stwalley. Photoassociative production and trapping of ultracold KRb molecules. *Phys. Rev. Lett.*, 93(24):243005, 2004.
- [8] J.M. Sage, S. Sainis, T. Bergeman, and D. DeMille. Optical production of ultracold polar molecules. *Phys. Rev. Lett.*, 94(20):203001, 2005.
- [9] K.-K. Ni, S. Ospelkaus, M. H. G. de Miranda, A. Peer, B. Neyenhuis, J. J. Zirbel, S. Kotochigova, P. S. Julienne, D. S. Jin, and J. Ye. A high phase-space-density gas of polar molecules. *Science*, 322:231, 2008.
- [10] J. Deiglmayr, A. Grochola, M. Repp, K. Mörtlbauer, C. Glück, J. Lange, O. Dulieu, R. Wester, and M. Weidemüller. Formation of ultracold polar molecules in the rovibrational ground state. *Phys. Rev. Lett.*, 101(13):133004, 2008.
- [11] S. Ospelkaus, K-K Ni, G. Quéméner, B. Neyenhuis, D. Wang, M.H.G. deMiranda, J.L. Bohn, J. Ye, and D.S. Jin. Controlling the hyperfine state of rovibronic ground-state polar molecules. *Phys. Rev. Lett.*, 104:030402, 2010.
- [12] M.H.G. de Miranda, A. Chotia, B. Neyenhuis, D. Wang, G. Quéméner, S. Ospelkaus, J.L. Bohn, J. Ye, and D.S. Jin. Controlling the quantum stereodynamics of ultracold bimolecular reactions. *Nat. Phys.*, 7:502–507, 2011.
- [13] A. Griesmaier, J. Werner, S. Hensler, J. Stuhler, and T. Pfau. Bose-Einstein condensation of chromium. *Phys. Rev. Lett.*, 94(16):160401, 2005.
- [14] Q. Beaufils, R. Chicireanu, T. Zanon, B. Laburthe-Tolra, E. Maréchal, L. Vernac, J.-C. Keller, and O. Gorceix. All-optical production of chromium Bose-Einstein condensates. *Phys. Rev. A*, 77(6):061601, 2008.
- [15] J.J. McClelland and J.L. Hanssen. Laser cooling without repumping: A magneto-optical trap for erbium atoms. *Phys. Rev. Lett.*, 96(14):143005, 2006.
- [16] K. Aikawa, A. Frisch, M. Mark, S. Baier, A. Rietzler, R. Grimm, and F. Ferlaino. Bose-Einstein condensation of erbium. *Phys. Rev. Lett.*, 108(21):210401, 2012.
- [17] M. Lu, S.H. Youn, and B.L. Lev. Trapping ultracold dysprosium: A highly magnetic gas for dipolar physics. *Phys. Rev. Lett.*, 104(6):063001, 2010.
- [18] S.H. Youn, M. Lu, U. Ray, and B.L. Lev. Dysprosium magneto-optical traps. *Phys. Rev. A*, 82(4):043425, 2010.
- [19] S.H. Youn, M. Lu, and B.L. Lev. Anisotropic sub-Doppler laser cooling in dysprosium magneto-optical traps. *Phys. Rev. A*, 82(4):043403, 2010.
- [20] M. Lu, S.H. Youn, and B.L. Lev. Spectroscopy of a narrow-line laser-cooling transition in atomic dysprosium. *Phys. Rev. A*, 83(1):012510, 2011.
- [21] M. Lu, N.Q. Burdick, S.H. Youn, and B.L. Lev. Strongly dipolar Bose-Einstein condensate of dysprosium. *Phys. Rev. Lett.*, 107(19):190401, 2011.
- [22] D. Sukachev, A. Sokolov, K. Chebakov, A. Akimov, S. Kanorsky, N. Kolachevsky, and V. Sorokin. Magneto-optical trap for thulium atoms. *Phys. Rev. A*, 82(1):011405, 2010.
- [23] D. Sukachev, K. Chebakov, A. Sokolov, A. Akimov, N. Kolachevsky, and V. Sorokin. Laser cooling of thulium atoms. *Opt. Spec.*, 111(4):633–638, 2011.
- [24] V.A. Dzuba and V.V. Flambaum. Theoretical study of some experimentally relevant states of dysprosium. *Phys. Rev. A*, 81(5):052515, 2010.
- [25] V.A. Dzuba, V.V. Flambaum, and B.L. Lev. Dynamic polarizabilities and magic wavelengths for dysprosium. *Phys. Rev. A*, 83(3):032502, 2011.

- [26] M. Tomza. Prospects for ultracold polar and magnetic chromium–closed-shell-atom molecules. *Phys. Rev. A*, 88(1):012519, 2013.
- [27] A. Kozlov, V.A. Dzuba, and V.V. Flambaum. Prospects of building optical atomic clocks using Er I or Er III. *Phys. Rev. A*, 88(3):032509, 2013.
- [28] U.I. Safranova, A.S. Safranova, and P. Beiersdorfer. Contribution of the $4f$ -core-excited states in determination of atomic properties in the promethium isoelectronic sequence. *Phys. Rev. A*, 88(3):032512, 2013.
- [29] B.K. Newman, N. Brahms, Y.S. Au, C. Johnson, C.B. Connolly, J.M. Doyle, D. Kleppner, and T.J. Greytak. Magnetic relaxation in dysprosium-dysprosium collisions. *Phys. Rev. A*, 83(1):012713, 2011.
- [30] A. Frisch, K. Aikawa, M. Mark, F. Ferlaino, E. Berseneva, and S. Kotochigova. Hyperfine structure of laser-cooling transitions in fermionic erbium-167. *Phys. Rev. A*, 88:032508, 2013.
- [31] C. Cohen-Tannoudji and K.W. Madison. *Annual Review of Cold Atoms and Molecules*. World Scientific, 2013.
- [32] Xi Chu, A. Dalgarno, and G.C. Groenenboom. Dynamic polarizabilities of rare-earth-metal atoms and dispersion coefficients for their interaction with helium atoms. *Phys. Rev. A*, 75(3):032723, 2007.
- [33] D.R. Lide. *CRC handbook of chemistry and physics*. CRC press, 2012.
- [34] R.D. Cowan. *The theory of atomic structure and spectra*, volume 3. University of California Press, 1981.
- [35] B.R. Judd. Complex atomic spectra. *Rep. Prog. Phys.*, 48(7):907–954, 1985.
- [36] J.F. Wyart and J.E. Lawler. Theoretical interpretation and new energy levels in Er II. *Phys. Scr.*, 79(4):045301, 2009.
- [37] E.A. Den Hartog, J.P. Chisholm, and J.E. Lawler. Radiative lifetimes of neutral erbium. *J. Phys. B*, 43(15):155004, 2010.
- [38] J.E. Lawler, J.F. Wyart, and E.A. Den Hartog. Atomic transition probabilities of Er i. *J. Phys. B*, 43(23):235001, 2010.
- [39] Yu. Ralchenko, A.E. Kramida, and J. Reader. Team (2008). NIST atomic spectra database (version 3.1.5). *Natl. Inst. Standards Technol.*, 2009.
- [40] R. Grimm, M. Weidemüller, and Y.B. Ovchinnikov. Optical dipole traps for neutral atoms. *Adv. At. Mol. Opt. Phys.*, 42:95–170, 2000.
- [41] P.W. Langhoff, S.T. Epstein, and M. Karplus. Aspects of time-dependent perturbation theory. *Rev. Mod. Phys.*, 44(3):602, 1972.
- [42] R. Vexiau, N. Bouloufa, M. Aymar, J.G. Danzl, M.J. Mark, H.C. Nägerl, and O. Dulieu. Optimal trapping wavelengths of Cs_2 molecules in an optical lattice. *Eur. Phys. J. D*, 65(1-2):243–250, 2011.
- [43] N.L. Manakov, V.D. Ovsianikov, and L.P. Rapoport. Atoms in a laser field. *Phys. Rep.*, 141(6):320–433, 1986.
- [44] J.R.P. Angel and P.G.H. Sandars. The hyperfine structure Stark effect. I. Theory. *Proc. R. Soc. London A*, 305(1480):125–138, 1968.
- [45] W.C. Martin, R. Zalubas, and L. Hagan. Atomic energy levels—the rare-earth elements. *Stand. Ref. Data Ser. (National Bureau of Standards, US)*, 60:332–338, 1978.
- [46] H.D. Kronfeldt, D. Ashkenasi, S. Kröger, and J.F. Wyart. Fine and hyperfine structure for $4f^{11}5d6s6p$ in Er I. *Phys. Scr.*, 48(6):688–698, 1993.
- [47] J.F. Wyart. Theoretical interpretation of the Nd II spectrum: odd parity energy levels. *Phys. Scr.*, 82(3):035302, 2010.
- [48] L. Brewer. Energies of the electronic configurations of the singly, doubly, and triply ionized lanthanides and actinides. *J. Opt. Soc. Am.*, 61(12):1666–1682, 1971.
- [49] L. Brewer. *Systematics of the Properties of the Lanthanides*. Ed. S.P. Sinha, D Reidel Publ. Co, 1983.
- [50] C. McGuinness. *Los Alamos version of the Cowan codes for Linux*. Available at <http://www.tcd.ie/Physics/people/Cormac.McGuinness/Cowan/>, 2009.
- [51] A. Kramida. *PC version of the Cowan codes*. Available at <http://das101.isan.troitsk.ru/COWAN>, 2010.
- [52] S. Kotochigova and A. Petrov. Anisotropy in the interaction of ultracold dysprosium. *Phys. Chem. Chem. Phys.*, 13(42):19165–19170, 2011.
- [53] S.G. Porsev, A. Derevianko, and E.N. Fortson. Possibility of an optical clock using the $6^1s_0 \rightarrow 6^3p_0$ transition in $^{171,173}\text{Yb}$ atoms held in an optical lattice. *Phys. Rev. A*, 69(2):021403, 2004.
- [54] M. Takamoto, F.L. Hong, R. Higashi, and H. Katori. An optical lattice clock. *Nature*, 435(7040):321–324, 2005.
- [55] A.D. Ludlow, T. Zelevinsky, G.K. Campbell, S. Blatt, M.M. Boyd, M.H.G. De Miranda, M.J. Martin, J.W. Thomsen, S.M. Foreman, J. Ye, et al. Sr lattice clock at 1×10^{-16} fractional uncertainty by remote optical evaluation with a Ca clock. *Science*, 319(5871):1805–1808, 2008.
- [56] B. Neyenhuis, B. Yan, S.A. Moses, J.P. Covey, A. Chotia, A. Petrov, S. Kotochigova, J. Ye, and D.S. Jin. Anisotropic polarizability of ultracold polar $^{40}\text{K}^{87}\text{Rb}$ molecules. *Phys. Rev. Lett.*, 109(23):230403, 2012.